

Graph Optimization Approach to Localization with IMU and Ultra-Wideband Measurements

Chen Wang[†], *Xu Fang[†], Thien-Minh Nguyen, Lihua Xie *Fellow, IEEE*

Abstract—An ultra-wideband (UWB) aided localization system is presented. Existing filter-based methods using UWB need kinetic model which is generally hard to obtain because of the complex structure of robots. This paper proposes a graph optimization approach to localization with inertial measurement unit (IMU) and UWB measurements which converts the localization problem into an optimization problem on Lie-Manifold, so that kinetic model can be avoided. This method makes full use of measurement data to localize a robot with acceptable computational complexity. It is achieved by minimizing the trajectory error based on several constrained equations arising from different types of sensor measurements. Our first contribution is graph realization in Manifold instead of Euclidean space for UWB-based systems, and new type of edge is defined and created in order to apply exiting graph optimization tool. Our second contribution is online approach that enables this approach to robots with ultra-low power processor. Experiments under a variety of scenarios verify the stability of this method and demonstrate that the algorithm achieves a much higher localization accuracy than the filter-based methods.

Index Terms—Ultra-Wideband (UWB), Inertial Measurement Unit (IMU), Localization, Lie-Manifold, Unmanned Aerial Vehicle (UAV).

I. INTRODUCTION

LOCALIZATION accuracy and speed play an important role in robot-related applications, such as path following, target searching and obstacle avoidance. The success of such applications relies on the localization algorithm and performance of localization-related sensors. However, some existing localization technologies are difficult or expensive to be deployed directly. For example, the widely-used Global Positioning System (GPS) can only be applied in outdoor environment due to the non-line of sight (NLOS) blockage in indoor environment. The vision-based real-time simultaneous localization and mapping (SLAM) technologies [1], [2], [3] have an unacceptable drift without odometer correction and need significant computational resources for dense mapping, which are not suitable for ultra-low power processor. The WiFi-based localization [4], [5], [6] has the problem of large fluctuations caused by the variation of signals and its unsatisfactory accuracy makes it inapplicable to robots such as unmanned aerial vehicle (UAV). Motion capture systems can provide millimeter level of accuracy and focus on challenging tasks such as formation and swarming [7], [8]. But they are very expensive and only applicable to small-scale spaces. An alternative method which utilizes the ultra-

The authors are with School of Electrical and Electronic Engineering, Nanyang Technological University, Singapore (e-mail: wang.chen@zoho.com, *fa0001xu@e.ntu.edu.sg, e150040@e.ntu.edu.sg, elhxie@ntu.edu.sg).

[†]Chen Wang and Xu Fang are joint first authors.

wideband communication has attracted researchers' attention due to its robustness to multipath and non-line of sight effects. This characteristic brings about high speed communication and ranging measurement. Robot carrying a UWB module is able to calculate its relative distances to other UWB modules (referred to as anchors) by measuring the time of arrival (TOA), which is then used for estimating its own position. The existing results using UWB for localization can be found in [9], [10], [11], [12], [13]. For UWB-based localization, the robots [14] are able to locate themselves by using a set of fixed anchors, and an extended aerodynamic model for localization under the assumption of no wind. The specification of a time of flight-based ranging protocol [15] is proposed for localization without involving a localization server. Cooperative UWB localization tackling the trade-off between accuracy and delay is considered in [16], which derives lower bounds on UWB positioning accuracy. For localization-related applications, the localization is applied to swarms of robots in [17], which utilizes tessellated maps that associate probabilistic error models for localization. The capability of supporting multi-UAV formation is presented in [18]. But this localization system needs to be fused with other sensors to obtain altitude estimation. Without fixed-anchors, a small number of anchors mounted on the moving robots can be used for target tracking[19], which only require that the target be equipped with a UWB transceiver. One potential application of UWB is the relative localization for moving robots in GPS-denied environments, which is the key technology for applications such as relative position information based formation and swarming algorithms. To improve the accuracy of UWB-based localization, some papers focus on the problem of optimal sensor placement [20], [21], [22]. The common conclusion is that the anchors should be spread evenly about the robot.

The current UWB-based localization methods are mainly based on Kalman filters such as Extended Kalman Filter (EKF) and Unscented Kalman Filter (UKF) [23], [24], [25]. The EKF can provide real-time vehicle position updates which relies on linear dynamic models. UKF is an improvement over EKF. Deterministic sampling approach is used to pick a minimal set of sample points (sigma points) around the mean. These sigma points are then propagated through the non-linear model, from which a new mean and covariance estimates are formed and a better estimation of the state can be obtained based on these propagated sigma points. Other methods are Particle filters and Non-linear regression [18], [26], [27]. Particle filters uses a genetic mutation-selection sampling approach for estimation, with a set of particles to represent the posterior distribution of stochastic process. Non-

linear regression is a form of regression analysis which models observational data by a function.

The common characteristic of these methods is that they need kinetic model. However, an obvious problem is that kinetic model is always nonlinear and also hard to obtain due to the complex structure of robots. The simplified or linearized kinetic model will bring unpredictable localization error. Also, these methods only utilize current measurement and a priori estimate for each estimation, which will diverge if the signal is lost for short time.

Considering above drawbacks, a localization method is presented in this paper to improve the accuracy and stability of UWB-based localization. Inspired by the theory of Lie group and Lie algebra, the robot or anchor poses at each time instant can be regarded as a rigid transformation in 3-D space, resulting in several constrained equations. Therefore, the task of localization becomes an optimization problem on Lie-Manifolds with various constraints due to different kinds of measurements. A remarkable advantage of the proposed method is that the kinetic model of the robot is avoided and the position of the robot can be estimated by calculating the optimal solution to the optimization problem. It is worth noting that at each time instant the newly added transformations and constrained equations are able to correct the previous estimate of position. The proposed method is robust to short lost in signal because it utilizes not only current measurements but also previous measurements to avoid divergence. This characteristic adds more constraints to estimation, which will improve the estimation accuracy.

II. RELATED WORK

The literature review only focuses on localization technologies that are most closely related to our work.

A. Simultaneous Localization and Mapping

The similar technology for Lie-Manifolds-based localization is used in SLAM technology [28], [29], [30], which not only builds constrained equations between adjacent frames, but also between landmarks and frames. The landmarks in SLAM serve as similar function as anchors in UWB-based localization. These constrained equations among frames and landmarks mainly describe their pose relationships.

For camera-based system, iterative closest point is one of the most widely used algorithms which need powerful GPU to process pose relationships. Feature-based [31], [32] and direct methods [33], [34] use iterative methods such as Gauss-Newton to match the images for monocular, stereo cameras and depth cameras. The deep learning based SLAM [35], [36] also need iterative solutions to adjust the weights in neural networks. A non-iterative SLAM is presented in [37] to reduce the computational requirements dramatically, which demonstrates a new objective function with closed-form solution. The rotational motions are decoupled from translational motions. The transnational motion model can be obtained by single key-frame training. Then robot motions are obtained by recoupling the estimation in rotational and translational spaces.

Compared with UWB-based localization, camera-based systems have long range and high resolution, but [38] the computation cost is considerably high so that it can not be applied to robots with ultra-low power processor. In addition, the good visual features are difficult to extract and match, and SLAM has an unacceptable drift without loop closure detection. Other SLAM systems such as laser-based and sonar-based systems depend on inertial sensors. The small errors in inertial sensors can lead to large localization errors.

It is well-known that graph optimization approaches are superior to filtering approaches in terms of robustness. We propose to apply this technique to the problem of localization using UWB-IMU data fusion. The relationships of frames and landmarks in SLAM are pose constraints. But the relationships in UWB-based systems include distance relationship between robot and anchors, which is a challenge for applying existing graph optimization tool to UWB-based systems because it doesn't include this type of relationship in the existing open-source optimization libraries. The new functions need to be defined and created in order to apply existing graph optimization tool to UWB-based systems. This paper aims to combine the advantages of graph optimization method and good performance of UWB sensor, and propose a novel localization structure for UWB-based localization which not only has less computation cost than that in SLAM but also has better localization accuracy than existing UWB-based localization methods.

B. Graph Realization

The literature on graph realization problem focuses on finding Euclidean positions for the vertices of a graph given a set of edge lengths, which is different from SLAM. A theory of network localization in terms of graph rigidity theory is proposed [39] to find a unique realization. However, alternative incorrect realizations may arise under the presence of measurement noise. [40] proposes a noise model to get the noise characteristics of UWB measurements. Then uses a maximum likelihood estimator for prelocalization in Cartesian coordinates and obtaining noise covariance matrix that is used in Kalman filter to update the state estimation recursively. [41] proposes a method for calibration-free, infrastructure-free localization in sensor networks. The generalization of classical multidimensional scaling algorithm is proposed to account for measurements and this method circumvents a-priori calibration. Similarly, several works addresses the geometric relations between robots and anchors [42], [43].

Compared with these UWB-based graph realizations, our approach exploits graph realization in Manifold instead of Euclidean space. The poses instead of translations of robot are used to build constrained equations directly between robot and anchors. The graph realization in Manifold brings better localization accuracy than that in Euclidean space because graph optimization approaches are superior to filtering approaches in terms of robustness.

UWB localization may be trapped in NLOS scenarios that induce multi-path signal components. The methods for this problem can be categorized into two groups: those that only

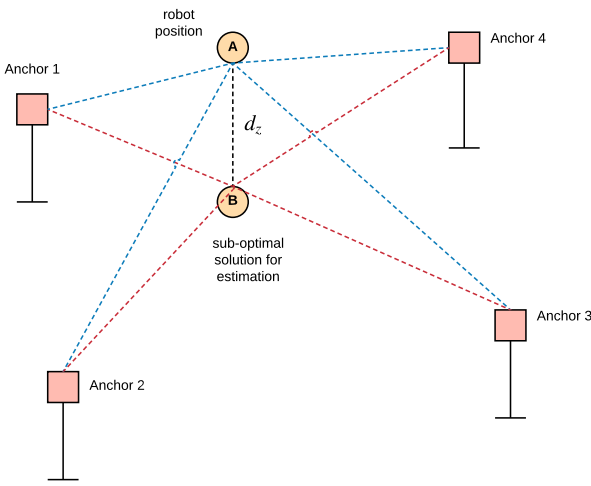


Fig. 1. The robot is at position A , but the estimation is at position B which has the same distances away from four anchors as at position A .

use LOS measurements [44], [45], and those that use both NLOS and LOS measurements [46], [47]. Our approach is to design an outlier rejector that rejects the NLOS measurements and only uses LOS measurements for localization.

C. Contributions

In contrast to existing UWB-based localization methods, the novelty of our approach is summarized as follows: (i) we do not need kinetic model for UWB-based localization, which is different with filtering-based localization methods, (ii) we exploit graph realization in Manifold instead of Euclidean space and new type of edge (distance edge) is defined and created in order to apply existing graph optimization tool to UWB-based systems, (iii) A flexible moving window is designed to decrease the computation, which enables this approach to robots with ultra-low power processor, (iv) Smooth edge between adjacent robot poses and its covariance matrices are defined and designed to improve the possibility of converging to optimal solutions. The existing algorithms have incompatible accuracy in altitude without adding other sensors such as Lidar sensor for estimating altitude, which is a persist issue. The reason for this phenomenon is shown by Fig. 1. The robot is at position A , but the estimation is at position B which is a sub-optimal solution because it has the approximate distances away from four anchors as at position A . This phenomenon will cause big estimation error along the altitude z . One possible way to solve this problem is to add more anchors or place one anchor on the ceiling. But for outdoor environment, it is difficult to place anchor on the ceiling.

An remarkable advantage of our approach is that the accuracy in altitude enables UWB-based localization to 3D space application in outdoor environment. The simplified or linearized kinetic model will bring unpredictable localization error. Compared with existing UWB-based localization methods that only utilize current measurement and a priori estimate for each estimation based on simplified or linearized kinetic model, our approach do not need kinetic model and utilizes not

only current measurements but also previous measurements to avoid divergence. This character adds more constraints to estimation, which brings better estimation accuracy in altitude under the same conditions. The main contributions of this paper are:

- 1) An novel online algorithm for UWB-based localization. The UWB and IMU sensor measurements are fused for graph realization, which is different from existing UWB-IMU data fusion using filter-based localization;
- 2) A framework for UWB-based localization using Lie Manifold optimization method. This framework is not only suitable for UWB and IMU based localization, but also can be extended to applications with other sensors such as WiFi and optical flow sensors;
- 3) The design of outlier rejector. Outlier rejector is proposed for rejecting NLOS measurements, which enables this approach to NLOS environment.
- 4) The design of flexible moving window. The flexible moving window decreases the computation and uses previous and newly measurements for localization. The proposed method is robust to short lost in signal because it uses previous and current measurements for localization instead of only using a priori estimate and current measurement in filtering-based methods. Moreover, at each time instant the newly added transformations and constrained equations are able to correct the previous estimate of position.
- 5) The implementation of the UWB-based localization method for unmanned aerial vehicles. Sensor data are integrated into a ROS-based robotic localization system. The experiment results verify the higher localization accuracy compared with traditional localization methods, especially in altitude.

It is worth noting that this technology is being commercialized because of its advantage in localization accuracy without adding other sensors such as Lidar sensor for estimating altitude. An technological company in Singapore is using this technique for aircraft inspection.

III. PRELIMINARY

In this section, a summary of relevant mathematical concepts about 3D transformation are presented.

A. Manifold, Lie group and Lie algebra

Let $M \in \mathbb{R}^n$ be connected, and be a family such that for a given $d \in \mathbb{N}$:

- 1) U_α is an open subset of M .
- 2) $\psi_\alpha: U_\alpha \rightarrow V_\alpha$ is a homeomorphism to an open subset $V_\alpha \in \mathbb{R}^d$.
- 3) If $U_\alpha \cap U_\beta \neq \emptyset$, the transition map $\psi_\alpha \circ \psi_\beta^{-1}$ is:
 $\psi_\beta(U_\alpha \cap U_\beta) \rightarrow \psi_\beta(U_\alpha \cap U_\beta)$ is C^k diffeomorphism.

Then (M, Γ) is called a manifold [48].

Manifold is a topological space that locally resembles Euclidean space near each point.

A group is an algebraic structure consisting of a set of elements equipped with an operation that combines any two

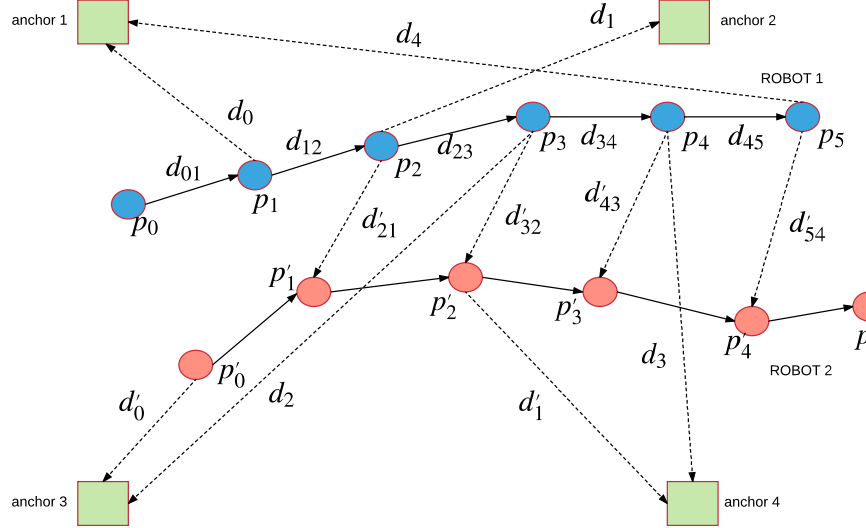


Fig. 2. Localization system used for constructing constrained equations are shown in this figure. Two robots move in 3-D space and four anchors are placed in fixed position. Each robot is equipped with UWB module.

elements to form a third element. The group SE(3) is Lie group [48] which is a smooth manifold. Considering the robot motion in 3D space, poses of robot can be regarded as rigid transformation (such as SE(3) in 3D space). The element of SE(3) can be shown by:

$$\mathbf{P} = \begin{bmatrix} \mathbf{R}_r & \mathbf{t} \\ \mathbf{0} & 1 \end{bmatrix} \in \text{SE}(3), \quad \mathbf{R}_r \in \text{SO}(3), \quad \mathbf{t} \in \mathbb{R}^3, \quad (1)$$

where \mathbf{P} is transformation, \mathbf{R}_r is rotation matrix and \mathbf{t} is translation vector. The elements in rotational group SO(3) are orthogonal matrices. The exponential map takes the Lie algebra $\mathfrak{so}(3)$ to rotation group SO(3) shown as following:

$$\begin{aligned} \omega &= (\omega_1, \omega_2, \omega_3)^T \in \mathbb{R}^3, \\ \omega_{\times} &= \begin{bmatrix} 0 & -\omega_3 & \omega_2 \\ \omega_3 & 0 & -\omega_1 \\ -\omega_2 & \omega_1 & 0 \end{bmatrix} \in \mathfrak{so}(3), \\ \mathbf{R}_r &= \exp(\omega_{\times}) \in \text{SO}(3), \end{aligned} \quad (2)$$

where ω_{\times} is skew symmetric matrices which belong to Lie algebra $\mathfrak{so}(3)$. The ω_{\times} is determined by vector ω which is often used to represent Lie algebra ω_{\times} . So the rotation matrix \mathbf{R}_r can be mapped into vector space ω . Similarly, the relationship between Lie algebra $\mathfrak{se}(3)$ and Lie group SE(3) is shown by:

$$\begin{aligned} \epsilon &= (\omega, \mathbf{u})^T \in \mathbb{R}^6, \quad \omega, \mathbf{u} \in \mathbb{R}^3, \\ \epsilon_{\times} &= \begin{bmatrix} \omega_{\times} & \mathbf{u} \\ \mathbf{0} & 0 \end{bmatrix} \in \mathfrak{se}(3), \\ \mathbf{P} &= \exp(\epsilon_{\times}) \in \text{SE}(3). \end{aligned} \quad (3)$$

Then definition of $\log_{\text{SE}(3)}(\cdot)$ is designed by

$$\log_{\text{SE}(3)}(\exp(\epsilon_{\times})) = \epsilon. \quad (4)$$

B. Operator for Lie-groups

The Lie group SE(3) is a kind of manifold, which consists of rotation matrix and translation vector. The translation vector \mathbf{t}

forms a Euclidean space but the rotation matrix \mathbf{R}_r span over non-Euclidean space. So conventional optimization methods applied in Euclidean space can not solve optimization problem on Lie-Manifolds. In order to use conventional optimization methods, manifold need to be mapped into Euclidean space. From (3), we can know $\epsilon \in \mathbb{R}^6$ is the corresponding vector mapped from transformation \mathbf{P} in 3D space. So group SE(3) can be mapped into vector space which is Euclidean space.

Operator \oplus is introduced to build the relationship between transformations. For example, for the two transformations $\mathbf{P}_1, \mathbf{P}_2 \in \text{SE}(3)$, corresponding vectors are $\epsilon_1, \epsilon_2 \in \mathbb{R}^6$. The transformation \mathbf{M} moving \mathbf{P}_1 to \mathbf{P}_2 can be represented by $\mathbf{M} = \mathbf{P}_1^{-1} * \mathbf{P}_2$, and mathematical relation among ϵ_1, ϵ_2 and ϵ_M is expressed by operator \oplus :

$$\epsilon_2 = \epsilon_1 \oplus \epsilon_M = \log_{\text{SE}(3)}(\exp(\epsilon_{1\times}) * \exp(\epsilon_{M\times})). \quad (5)$$

This kind of mapping is not unique. We choose (5) for localization in this paper. The $\epsilon_{1\times}$ and $\epsilon_{M\times}$ can be obtained using (3). The details of (5) are shown in next section.

IV. LOCALIZATION SYSTEM STRUCTURE

Given two transformations $\mathbf{P}_1, \mathbf{P}_2 \in \text{SE}(3)$, their corresponding rotation matrices $\mathbf{R}_{r1}, \mathbf{R}_{r2}$ and translation vectors $\mathbf{t}_1 = (t_{1x}, t_{1y}, t_{1z})^T, \mathbf{t}_2 = (t_{2x}, t_{2y}, t_{2z})^T$, three kinds of measurement variables are given by:

- 1) Transformation measurement variable $\hat{\mathbf{z}}_k \in \text{SE}(3)$:

$$\hat{\mathbf{z}}_k = \mathbf{P}_1^{-1} \cdot \mathbf{P}_2 = \begin{bmatrix} \mathbf{R}_{r1} & \mathbf{t}_1 \\ \mathbf{0} & 1 \end{bmatrix}^{-1} \cdot \begin{bmatrix} \mathbf{R}_{r2} & \mathbf{t}_2 \\ \mathbf{0} & 1 \end{bmatrix}. \quad (6)$$

- 2) Translational measurement variable $\hat{\mathbf{z}}_k \in \mathbb{R}^3$ and its elements variable $\hat{z}_k \in \mathbb{R}$:

$$\hat{\mathbf{z}}_k = \mathbf{t}_2 - \mathbf{t}_1, \quad (7)$$

with its elements $\hat{z}_k \in \mathbb{R}$:

$$\hat{z}_k = t_{2x} - t_{1x}, \quad t_{2y} - t_{1y}, \quad t_{2z} - t_{1z}. \quad (8)$$

Given a measurement function $\hat{\mathbf{y}}_k = \mathbf{h}_k(\hat{\mathbf{z}}_k) \in \mathbb{R}^L$, $\hat{\mathbf{y}}_k$ is predicted measurement. After getting the real measurement \mathbf{y}_k from sensors, a constrained equation can be expressed as $\mathbf{E}_k = \mathbf{f}(\hat{\mathbf{y}}_k, \mathbf{y}_k)$.

In 3-D space, three kinds of measurement functions are designed as following:

- 1) Transformation measurement function.

$$\mathbf{h}_k(\hat{\mathbf{z}}_k) = \log_{SE(3)}(\hat{\mathbf{z}}_k), \quad (9)$$

where $\mathbf{h}_k(\hat{\mathbf{z}}_k) \in \mathbb{R}^6$, $\hat{z}_k \in SE(3)$.

- 2) Translational measurement function.

$$\mathbf{h}_k(\hat{\mathbf{z}}_k) = \hat{\mathbf{z}}_k, \quad \hat{\mathbf{z}}_k \in \mathbb{R}^3, \quad (10)$$

with its elements:

$$h_k(\hat{z}_k) = \hat{z}_k, \quad \hat{z}_k \in \mathbb{R}. \quad (11)$$

- 3) Distance measurement function.

$$h_k(\hat{\mathbf{z}}_k) = \|\hat{\mathbf{z}}_k\|_2, \quad h_k(\hat{\mathbf{z}}_k) \in \mathbb{R}, \quad \hat{\mathbf{z}}_k \in \mathbb{R}^3. \quad (12)$$

Three kinds of measurement variables $\hat{\mathbf{z}}_k$ are mapped into vector spaces by the above measurement functions.

A GPS-denied localization system for robots is proposed with a small number of anchors placed in fixed positions, and each robot is equipped with one UWB module. In this system, each robot has an independent cost function used to estimate its positions. The localization algorithm uses measurements from UWB and IMU detailed below.

A. UWB integration

The UWB module can use either one-way communication or two-way communication to receive a distance measurement. UWB modules can also send data to each other.

The UWB ranging algorithm uses the TOA measurement (T_i) to calculate the distance [9]. The distance measurement $d \in \mathbb{R}$ can be obtained from the TOA measurement T_{ra} :

$$d = (T_{ra} - \Delta T_{ra}) \cdot c + n_{ra}, \quad (13)$$

where ΔT_{ra} is the processing time delay, c is the speed of light, and n_{ra} is the measurement noise. In order to use this ranging algorithm, robot and anchor clock need to be synchronized.

The constrained equation between robot translation \mathbf{t}_i and fixed anchor translation \mathbf{t}_i^{uwb} is designed based on (12):

$$E_{k,i}^r = e_{k,i}^{r,T} w_i^r e_{k,i}^r, \quad (14a)$$

$$e_{k,i}^r = d_i - \|\mathbf{t}_i - \mathbf{t}_i^{uwb}\|_2, \quad (14b)$$

where d_i is the measured distance between robot translation \mathbf{t}_i and fixed anchor translation \mathbf{t}_i^{uwb} . k is the time instant at which a measurement is acquired. w_i^r is a penalty term given by:

$$w_i^r = \frac{\iota^2}{\|\Omega_i^r\|_2^2 + \iota^2}, \quad (15)$$

where ι is a free-parameter and $\Omega_i^r \in \mathbb{R}$ is the variance of the distance measurement d_i . (14) only gives a constraint on a set of sparse points and fails to form a smooth trajectory. A constrained equation between adjacent translations (\mathbf{t}_i and \mathbf{t}_{i-1}) is needed to smooth the trajectory. The constrained equation for adjacent translations is designed as:

$$E_{k,i}^c = e_{k,i}^{c,T} w_i^c e_{k,i}^c, \quad (16a)$$

$$e_{k,i}^c = \|\mathbf{t}_i - \mathbf{t}_{i-1}\|_2, \quad (16b)$$

where w_i^c is penalty term shown as:

$$w_i^c = \frac{9\iota^2}{\|v_{max} \cdot \Delta T\|_2^2 + 9\iota^2}, \quad (17)$$

where ΔT is the time interval between \mathbf{t}_i and \mathbf{t}_{i-1} . v_{max} is the maximum velocity. This can be interpreted as the probabilistic distance between two consecutive transformations by applying the three-sigma rule under the assumption that the linear velocity of the robot follows a normal distribution.

Combining (14) and (16), an estimated trajectory \mathbf{t}^* can be obtained by the following optimization:

$$\mathbf{F}_{rc}(\mathbf{t}) = \sum_{k,i} (E_{k,i}^r + E_{k,i}^c), \quad (18a)$$

$$\mathbf{t}^* = \arg \min \mathbf{F}_{rc}(\mathbf{t}). \quad (18b)$$

B. IMU integration

IMU sensor [49] is used to obtain rotation information. The representation of orientation from IMU is quaternion.

The translation vector \mathbf{t} can be acquired by:

$$\begin{aligned} \mathbf{t}_w(T + \Delta T) &= \mathbf{t}_w(T) + \mathbf{v}_w(T)\Delta T + \frac{1}{2}\mathbf{a}_w(T)\Delta T^2, \\ \mathbf{a}_w(T) &= \mathbf{R}^T(T)\mathbf{a}_b(T) + \mathbf{g}_w + \eta(T), \end{aligned} \quad (19)$$

where T is the current time and $\mathbf{v}_w(T)$ is the velocity of robot, and \mathbf{a}_w is the linear acceleration in world frame. $\mathbf{a}_b(T)$ and \mathbf{R} are from IMU, which are the linear acceleration in body frame and rotation matrix, respectively. $\eta(T)$ is the environment noise and \mathbf{g}_w is the acceleration of gravity.

For adjacent transformations \mathbf{p}_i and \mathbf{p}_{i-1} (transformation is defined in (1)), the transformation constraint \mathbf{z}_k between \mathbf{p}_i and \mathbf{p}_{i-1} is designed as:

$$\mathbf{z}_k = \begin{bmatrix} \mathbf{R}_{i-1}^{-1} \mathbf{R}_i & \mathbf{R}_{i-1}^{-1} (\mathbf{t}_i - \mathbf{t}_{i-1}) \\ \mathbf{0} & 1 \end{bmatrix}. \quad (20)$$

The rotations \mathbf{R}_i and \mathbf{R}_{i-1} is obtained from IMU. The constrained equation between \mathbf{p}_i and \mathbf{p}_{i-1} is designed based on (9).

$$E_{k,i}^p = \mathbf{e}_{k,i}^{p,T} \mathbf{w}_i^p \mathbf{e}_{k,i}^p, \quad (21)$$

$$\mathbf{e}_{k,i}^p = \log_{SE(3)}(\mathbf{z}_k) - \log_{SE(3)}(\mathbf{p}_{i-1}^{-1} \mathbf{p}_i),$$

where matrix \mathbf{w}_i^p is term penalty shown as:

$$\mathbf{w}_i^p = \begin{bmatrix} \Omega_i^o & \mathbf{0} \\ \mathbf{0} & \Omega_i^t \end{bmatrix}, \quad (22)$$

with $\Omega_i^o \in \mathbb{R}^{3 \times 3}$ and $\Omega_i^t \in \mathbb{R}^{3 \times 3}$ being the covariance matrices of orientation and translation. Ω_i^t is a diagonal matrix

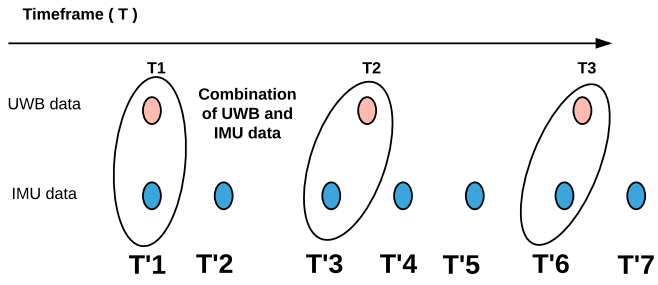


Fig. 3. IMU and UWB data are combined by a filter shown in the figure. At each UWB time instant (such as T1, T2, T3) we get a UWB measurement data. From IMU time instant (such as T'1, T'2, ..., T'6), we choose an IMU data whose time instant (such as T'1, T'3, T'6) is closest to the corresponding UWB time instant (T1, T2, T3). These chosen IMU data are regarded as approximate IMU data at time instant (T1, T2, T3).

with diagonal elements $\frac{9t^2}{\|v_{max} \cdot \Delta T\|_2^2 + 9t^2}$ if we can not obtain robot velocity.

If we can get robot velocity and acceleration from other sensors such as optical flow, the penalty term w_i^c in (17) and the diagonal elements in Ω_i^t can be designed as:

$$w_i^c = \frac{9t^2}{\|v_{i-1}(T)\Delta T + \frac{1}{2}a_{i-1}(T)\Delta T^2\|_2^2 + 9t^2}, \quad (23)$$

where v_{i-1} and a_{i-1} are robot velocity and acceleration in world frame.

Similarly, an estimated transformations p^* can be obtained:

$$\mathbf{F}_{rp}(\mathbf{p}) = \sum_{k,i} (E_{k,i}^r + E_{k,i}^p), \quad (24a)$$

$$\mathbf{p}^* = \arg \min \mathbf{F}_{rp}(\mathbf{p}). \quad (24b)$$

IMU and UWB measurement data cannot be acquired at the same time instant shown in Fig. 3. At each time instant T_i , we get a UWB measurement at position p_i ($i = 1, 2, \dots, n$), an IMU data whose time instant is closest to the UWB time instant T_i is considered as the approximate IMU data of the robot at UWB time instant T_i .

Some translations of robots can be known (such as start position and end position). For known robot translation $t_i = (t_x, t_y, t_z)^T$ obtained by some sensors, (11) is used to construct constrained equations for a known position:

$$e_{k,i}^n = \hat{t}_x - t_x; \quad e_{k,i}^n = \hat{t}_y - t_y; \quad e_{k,i}^n = \hat{t}_z - t_z, \quad (25)$$

where t_x , t_y and t_z are sensor measurements of known translations of robots.

C. Noise distribution

Gaussian distribution over transformations in Lie group G has a mean transformation $\mu \in G$ and covariance matrix $\Sigma \in \mathbb{R}^{k \times k}$ [50]. For a sample noise \tilde{x} which is from the Gaussian distribution in Lie space (μ, Σ) with mean μ satisfying

$$\tilde{x} = \exp(\epsilon_{\times}) \cdot \mu, \quad (26)$$

where ϵ_{\times} is from Gaussian distribution $\epsilon_{\times} \in N(0, \Sigma)$. For any $y \in G$, the transformed noise distribution $y \cdot \tilde{x}$ is

$$\begin{aligned} y \cdot \tilde{x} &= y \cdot \exp(\epsilon_{\times}) \cdot \mu = \exp(Adj_y \cdot \epsilon_{\times}) \cdot y \cdot \mu, \\ \epsilon_{\times} \in se(3), \exp(\epsilon_{\times}) &= \begin{bmatrix} \mathbf{R} & \mathbf{t} \\ \mathbf{0} & 1 \end{bmatrix} \in SE(3), \\ \exp(Adj_y) &= \begin{bmatrix} \mathbf{t} \times \mathbf{R} & \mathbf{R} \\ \mathbf{R} & 0 \end{bmatrix}. \end{aligned} \quad (27)$$

Then we can get the transformed noise distribution:

$$y \cdot \tilde{x} \in N(y \cdot x, Adj_y \cdot \sum \cdot Adj_y). \quad (28)$$

V. OPTIMIZATION ON LIE-MANIFOLDS

For the constrained equation shown in (14), (16) or (21), it is easy to get the Taylor expansion of $e_{k,i}^{\times}$ around the initial guess $\tilde{\epsilon}$,

$$e_{k,i}^{\times}(\tilde{\epsilon} + \Delta\epsilon) \simeq e_{k,i}^{\times}(\tilde{\epsilon}) + \mathbf{J}_k \Delta\epsilon, \quad (29)$$

where $e_{k,i}^{\times}$ represents $e_{k,i}^r$, $e_{k,i}^c$ or $e_{k,i}^p$, \mathbf{J}_k is Jacobian in $\tilde{\epsilon}$, $\Delta\epsilon$ is an increment, then the constraint equation becomes

$$\begin{aligned} E_{k,i}^{\times}(\tilde{\epsilon} + \Delta\epsilon) &= e_{k,i}^{\times}(\tilde{\epsilon} + \Delta\epsilon)^T \mathbf{w}_i^{\times} e_{k,i}^{\times}(\tilde{\epsilon} + \Delta\epsilon) \\ &\simeq \mathbf{c}_k + 2\mathbf{b}_k \Delta\epsilon + \Delta\epsilon^T \mathbf{H}_k \Delta\epsilon, \end{aligned} \quad (30)$$

where $\mathbf{b}_k = 2e_{k,i}^{\times T} \mathbf{w}_i^{\times} \mathbf{J}_k$, $\mathbf{c}_k = e_{k,i}^{\times T} \mathbf{w}_i^{\times} e_{k,i}^{\times}$, $\mathbf{H}_k = \mathbf{J}_k^T \mathbf{w}_i^{\times} \mathbf{J}_k$. Then, for cost functions in (18) or (24), we can get

$$\mathbf{F}(\tilde{\epsilon} + \Delta\epsilon) \simeq \mathbf{c} + 2\mathbf{b}^T \Delta\epsilon + \Delta\epsilon^T \mathbf{H} \Delta\epsilon, \quad (31)$$

where $\mathbf{c} = \sum \mathbf{c}_k$, $\mathbf{b} = \sum \mathbf{b}_k$ and $\mathbf{H} = \sum \mathbf{H}_k$. The increment $\Delta\epsilon$ for minimizing \mathbf{F} satisfies

$$\mathbf{H}\Delta\epsilon = -\mathbf{b}. \quad (32)$$

But if the matrix \mathbf{H} is not invertible, the increment $\Delta\epsilon$ cannot be acquired uniquely. The Levenberg-Marquardt [51] method introduces a damping factor $\lambda > 0$ to guarantee that the matrix \mathbf{H} is invertible.

$$(\mathbf{H} + \lambda \mathbf{I})\Delta\epsilon = -\mathbf{b}. \quad (33)$$

If the vector ϵ is from an Euclidean space, the optimized solution is

$$\epsilon^* = \tilde{\epsilon} + \Delta\epsilon, \quad \tilde{\epsilon} = \epsilon^*. \quad (34)$$

The matrix \mathbf{H} is sparse which can be decomposed by the LU decomposition or QR decomposition. The optimization process ((29)-(34)) continues until the maximum iteration number is reached or the cost function $\mathbf{F}(\epsilon)$ is close to zero.

But for the transformation \mathbf{P} , all the translation vectors \mathbf{t} form an Euclidean space but the rotation matrices \mathbf{R} span over a non-Euclidean space. This optimization method cannot find an optimal solution in a non-Euclidean space. An idea is that the group $SE(3)$ is regarded as Manifold, which can be mapped into Euclidean space ϵ by operator \oplus shown in (5). The operator \oplus for this optimization method is: $\text{Dom}(\tilde{\epsilon}) \times \text{Dom}(\Delta\epsilon) \rightarrow \text{Dom}(\epsilon)$:

$$\epsilon = \tilde{\epsilon} \oplus \Delta\epsilon. \quad (35)$$

The operator \oplus enables conventional standard optimization method to work on the manifold after replacing $+$ with \oplus [52]. A new constraint equation can be defined based on \oplus :

$$e_k(\tilde{\epsilon} \oplus \Delta\epsilon) \simeq e_k(\tilde{\epsilon}) + J_k \Delta\epsilon. \quad (36)$$

The jacobian matrix J_k can be calculated by

$$J_k = \frac{\partial e_k(\tilde{\epsilon} \oplus \Delta\epsilon)}{\partial \Delta\epsilon} \Big|_{\Delta\epsilon=0}. \quad (37)$$

Then the increment $\Delta\epsilon$ can be acquired by

$$\Delta\epsilon = -\left(\sum_{k=1}^m J_k^T \Omega_k J_k + \lambda \mathbf{I}\right)^{-1} \sum_{k=1}^m (2e_k(\tilde{\epsilon}) \Omega_k J_k). \quad (38)$$

The new optimized solution is obtained by operator \oplus :

$$\epsilon^* = \tilde{\epsilon} \oplus \Delta\epsilon. \quad (39)$$

Then Levenberg-Marquardt method can be used to find the optimal solution. The advantage of operator is that when group SE(3) is regarded as manifold, optimization on Lie-manifold does not need to deal with singularities or denormalized over-parameterizations. Also any conventional optimization method can be applied to find the optimal solution on a non-Euclidean space. Further, the Huber loss function can be applied to improve robustness of (30) against outliers:

$$\rho(x) = \begin{cases} x^2 & \text{if } |x| < k_c \\ 2k_c|x| - k_c^2 & \text{else} \end{cases}, \quad (40)$$

where $x = \sqrt{\mathbf{e}_{k,i}^\top \mathbf{w}_i^\top \mathbf{e}_{k,i}}$ and k_c is a constant. The Huber loss function is convex in a uniform neighborhood of its minimum $x = 0$. On the boundary of this uniform neighborhood, the Huber loss function has a differentiable extension to an affine function at points $x = k_c$ or $x = -k_c$.

VI. CONVERGENCE OF PROPOSED METHOD

A. Disadvantages of Filter-based Localization Methods

Kalman filter is an algorithm based on a kinetic model and measurement function, which produces estimation of unknown variables by using Bayesian inference and estimating a joint probability distribution over the variables.

One limitation is that the Kalman filter is designed for linear systems. When it is applied to a nonlinear system, the nonlinear system needs first to be linearized. The extended Kalman filter (EKF) is the nonlinear version of the Kalman filter which is based on the linearized model about an estimate of the current mean and covariance.

The algorithm of EKF consists of five equations, and the details of convergence analysis can be found in [53]. We can know that the convergence of EKF is mainly influenced by unmodeled dynamics, high-order nonlinear terms of Taylor expansion, system and measurement noises, and the accuracy of the initial estimate. The existence of the above factors might lead to a sub-optimal solution and even divergence.

The influence of high-order nonlinear terms are considered in the unscented Kalman filter (UKF) which does not need linearization. Deterministic sampling approach is used to pick a minimal set of sample points (called sigma points) around the mean. These sigma points are then propagated through the non-linear functions, from which a new mean and covariance estimates are then formed. But UKF also depends on a kinetic model and is influenced by unmodeled dynamics.

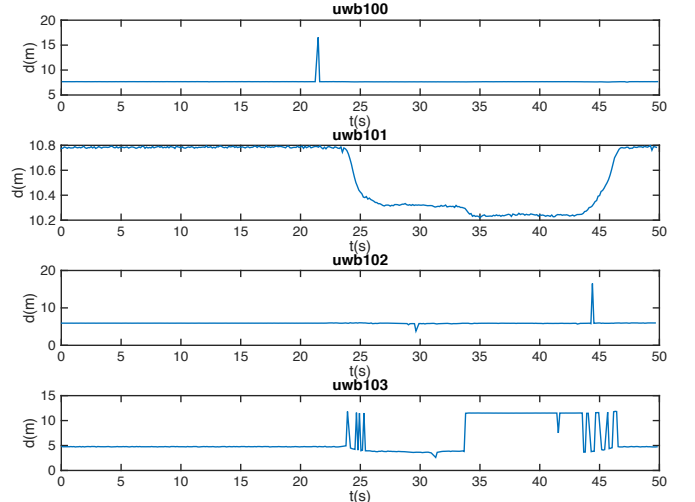


Fig. 4. Outlier rejector experiment.

B. Convergence of Proposed Method

From (31), the increment $\Delta\epsilon$ can be obtained by:

$$\min \mathbf{F}(\epsilon) = \mathbf{c}(\tilde{\epsilon} + \Delta\epsilon) + 2\mathbf{b}^T \Delta\epsilon + \Delta\epsilon^T \mathbf{H} \Delta\epsilon + M(\Delta\epsilon). \quad (41)$$

where $M(\Delta\epsilon)$ denotes high-order nonlinear terms and $\epsilon = \tilde{\epsilon} + \Delta\epsilon$.

From Lemma 2.4 in [51], λ is chosen such that $\lambda \mathbf{I} + \mathbf{H}$ is positive definite, then $\mu(\lambda) = \|\Delta\epsilon\|$ is monotonically decreasing and $\epsilon \rightarrow \epsilon^*$. From the cost function designed in Section IV, we can get the solution ϵ' that satisfies $\mathbf{F}(\epsilon') = 0$.

Considering the measurement noise, the cost function becomes:

$$\min \mathbf{F}(\epsilon) = F(\epsilon) + W. \quad (42)$$

where W is the noise. Suppose that $\epsilon' = \epsilon^* + \epsilon_d$ and $F(\epsilon^*) = 0$. ϵ^* is the optimal solution in the absence of noise. Then we get the following equation:

$$2\mathbf{b}^T \epsilon_d + \epsilon_d^T \mathbf{H} \epsilon_d \simeq -W, \quad (43)$$

where $\mathbf{b} = -(\lambda \mathbf{I} + \mathbf{H})\epsilon_d$. The Hessian matrix \mathbf{H} is real and symmetric. There exists an orthogonal matrix \mathbf{P} such that $\mathbf{P}^{-1} \mathbf{H} \mathbf{P} = \mathbf{H}_\Delta$. \mathbf{H}_Δ is a diagonal matrix and $\epsilon_m = \mathbf{P} \epsilon_d$. Thus,

$$\epsilon_m^T (-2\lambda \mathbf{I} - \mathbf{H}_\Delta) \epsilon_m \simeq -W, \quad (44)$$

where $\epsilon_m = [\epsilon_1, \epsilon_2, \dots, \epsilon_n]$,

$2\lambda \mathbf{I} + \mathbf{H}_\Delta = \text{diag}(m_1, m_2, \dots, m_n)$. (44) becomes:

$$m_1 \epsilon_1^2 + m_2 \epsilon_2^2 + \dots + m_n \epsilon_n^2 \simeq W. \quad (45)$$

If $m_1 = m_2 = \dots = m_n = M$, then the norm of the estimation error ϵ_m is:

$$\|\epsilon_m\|_2^2 \simeq \frac{W}{M}. \quad (46)$$

(46) shows that the estimation error ϵ_m is only related to measurement noises. As shown in Fig.2, robot moves from p_1 to p_4 and gets four distance measurements (d_0 to d_3) from anchor 1 to anchor 4. The four distance measurements can

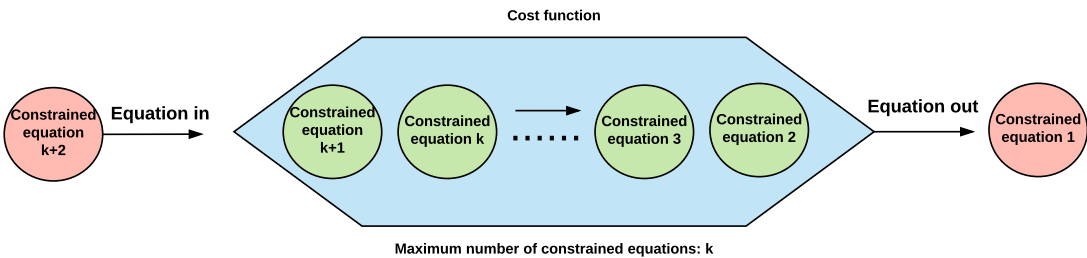


Fig. 5. The maximum number of equations for localization is designed to decrease the computation. When the number of equations get to maximum number of equations, then at each time instant when a new constrained equation (such as equation $(k+2)$) is added to the cost function, an old constrained equation (such as equation 1) is released.

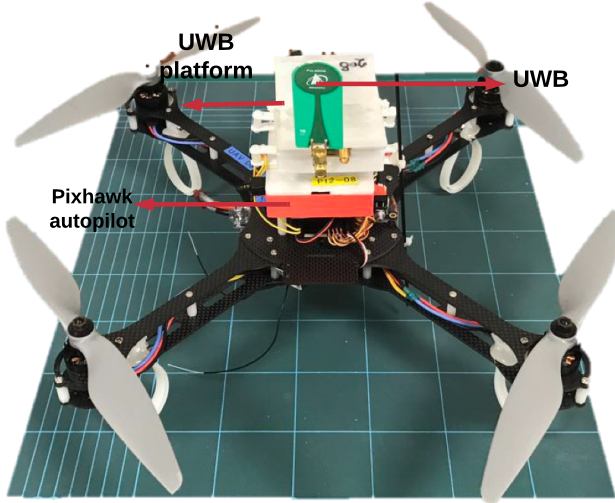


Fig. 6. UAV and UWB platform.

decide the center position p_{cen} of p_1 to p_4 . The solutions for p_1 to p_4 will converge to the adjacent domain of center position p_{cen} . Each position has at least three constrained equations, which contribute to finding the global optimal solution.

In contrast to existing UWB-based localization methods, the method proposed in this paper has the advantage that it does not require an kinetic model. At each time instant, the updated poses of the robot or anchors can be regarded as rigid transformations in 3-D space, and then constrained linear or nonlinear equations of the transformations are incorporated into the optimization. The position of the robot can be estimated by calculating the optimal solution to the optimization problem.

In the proposed method, at each time instant when a new measurement is added to the cost function, the updated optimal solution is obtained. In this way, newly added transformation and constrained equation are able to be used for correcting the previous estimation of position. Considering the computation of this method, a maximum number of constrained equations is set shown in Fig. 5. That is to say, at each time instant when a constrained equation of a new measurement is added to the cost function, an old constrained equation will be released.

In contrast to existing UWB-based localization methods based on EKF/UKF or nonlinear regression, the proposed

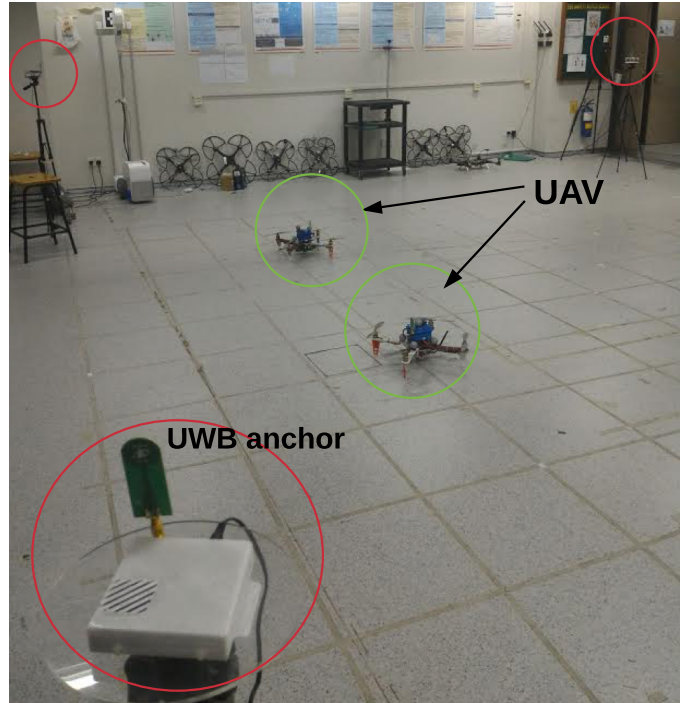


Fig. 7. Experiment environment.

localization method is of much better localization performance in terms of accuracy as demonstrated in the next section.

VII. IMPLEMENTATION

A. Particularities of UAV

In our experiment, localization of UAV in 3-D space is tested. Quadrotor UAV consists of four rotors which are configured in a cross shape as shown in Fig. 6. UAV is equipped with Pixhawk Autopilot which has two advanced processors (32-bit ARM Cortex M4 core with FPU and 32-bit failsafe co-processor). The co-processor has its own power supply even if the other one fails.

B. Particularities of UWB

UWB transceivers used in experiments are P440 modules from Time Domain shown in Fig. 6. The large bandwidth of UWB (from 3.1GHz to 5.3GHz) means that UWB signal is robust to multipath and can provide steady TOA and TDOA

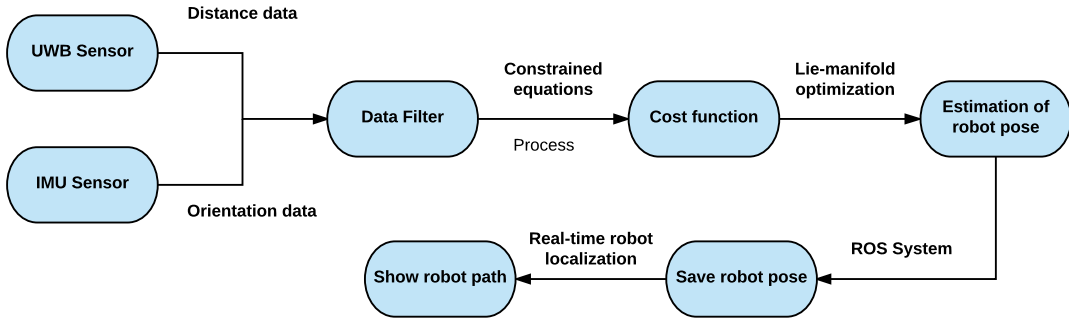


Fig. 8. Real-time localization system on ROS platform.

measurements. At each time instant, UWB can choose to act as requester or responder. A UWB module can send a ranging request and receive a ranging measurement from another UWB module.

The localization workflow is shown in Fig. 8. After getting and saving the estimates of the robot poses, a real-time estimated robot path can be obtained. UWB modules need to be calibrated before experiment. Denote the measured distance and the true distance by r and d , respectively. A linear function $r = ad + b$ can be used to calibrate the UWB distance measurement. Parameters a and b can be calculated given a set of samples $(d_i, r_i), (i = 1, 2, \dots, n)$. Least square is applied to obtain parameter estimation \hat{a} and \hat{b} .

$$\hat{a} = \frac{\sum_{i=1}^n (d_i - \bar{d})(r_i - \bar{r})}{\sum_{i=1}^n (d_i - \bar{d})}, \quad (47)$$

$$\hat{b} = \bar{r} - \hat{a}\bar{d}, \quad (48)$$

where \bar{r} and \bar{d} are the average distance measurement of r_i and true distance d_i , respectively.

C. Outlier Rejection

UWB localization may be trapped in NLOS scenarios that induce multi-path signal components. Our approach is to design an outlier rejector that rejects the NLOS measurements and only uses LOS measurements for localization.

At each time instant, robot stores estimation t_{i-1} at last time instant and receives a new distance measurement d_i from one fixed anchor (its translation is denoted by t_{ac}) at current time instant, the distance measurement d_i is considered as NLOS measurement if the following condition is satisfied:

$$|||t_{i-1} - t_{ac}||_2 - d_i| > 6v_{max} \cdot \Delta T, \quad (49)$$

where v_{max} is robot maximum velocity and ΔT is time interval of adjacent measurements. The NLOS measurement will be rejected and only LOS measurements are used for localization. From our experiments, robot is encouraged to be placed at a start position that doesn't have NLOS to get accurate initial estimation t_{i-1} .

An outlier rejector experiment with four anchors and one static robot is shown in Fig.4. The anchors positions for uwb100-uwb103 are (0, 0, -0.77), (6.13, 0, -5), (6.01, 8.07,

-0.79) and (0.11, 8.02, -5.02) respectively. The distance measurements of four anchors should be almost constant if there are no NLOS measurements. In this experiment, anchors uwb100-uwb103 have NLOS measurements. For example, anchor uwb103 has NLOS measurements from 23.2 second to 25.4 second and 33.8 second to 47.3 second respectively. The proposed method can reject these NLOS measurements and always calculate correct robot position (0.14, 7.63, -0.29) during 50 seconds. The outlier rejector is verified effectively for moving robot (UAV) by an technological company in Singapore.

VIII. EXPERIMENT

A. Experimental Environment

The UAV tests for 3-D localization were carried out in an area of square ($6m \times 6m$). Four UWB modules are placed in four different fixed positions to serve as anchors. The heights of anchors are also set differently because four non-coplanar points can construct a space. The four anchors are denoted by index 1, 2, 3, 4. The UAV is equipped with UWB and IMU sensors.

In this experiment, UAV will send requests to four anchors sequentially to get the distance measurements. The frequency of IMU (100.3 Hz) is about three times larger than that of UWB. The ground truth is provided by a Vicon system which has the accuracy of mm-level.

The UAV moved along a circle or a rectangle in a 2-D plane in our experiments. Localization in 2D plane is based on the cost function shown in (18), and 3D in (24). For translation, the mean and root mean square error (RMSE) are given by:

$$T_{mean} = \frac{1}{N} \sum_{i=1}^N ||e_i||, \quad (50)$$

$$T_{RMSE} = \sqrt{\frac{1}{N} \sum_{i=1}^N ||e_i - T_{mean}||}, \quad (51)$$

where e_i is the estimation error.

B. Parameter Selection

There are two important parameters needed to be set for the proposed localization algorithm. One is the maximum number of constrained equations. Considering the computation of the

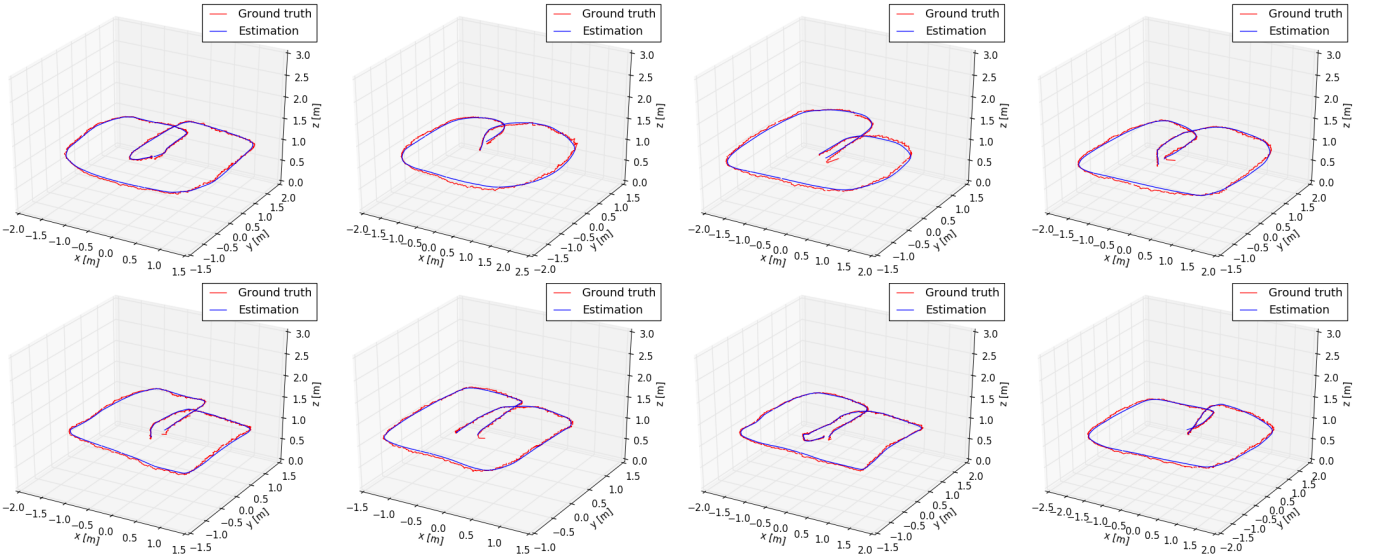


Fig. 9. UAV moved along a circle or rectangle in a 2-D plane. The red line is Ground truth from Vicon system, and the blue line is estimation combining UWB and IMU data.

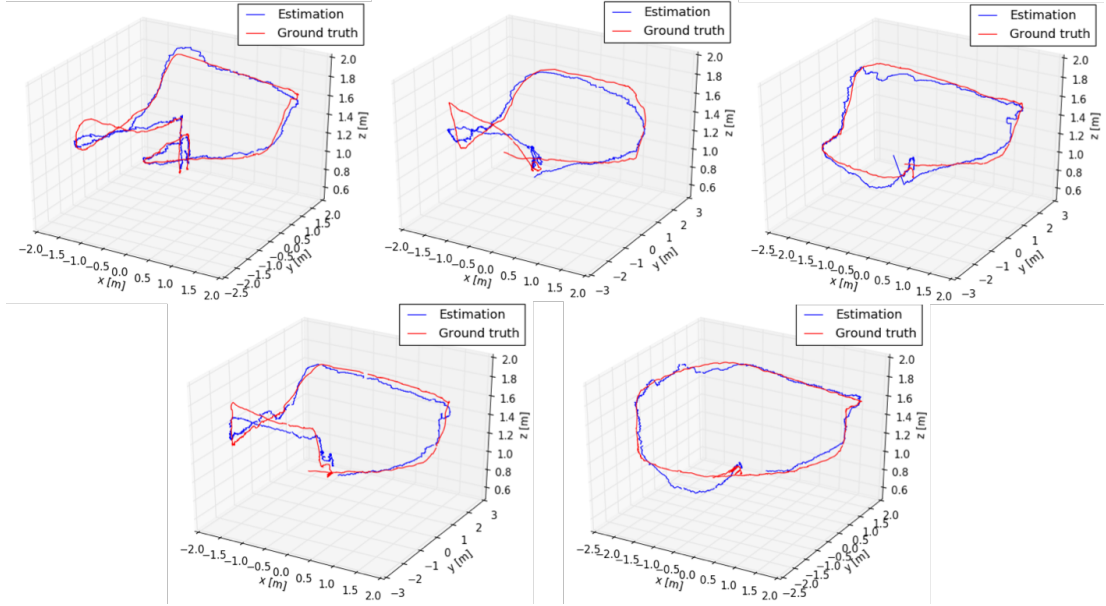


Fig. 10. UAV moved in 3-D space. The red line is Ground truth from Vicon system, and the blue line is the estimation combining UWB and IMU data.

TABLE I
POSITION ESTIMATED 2-NORM ERROR COMPARISON

UAV	UWB + IMU (2-D)	UWB + IMU (3-D)	EKF(3-D)	UKF(3-D)	Nonlinear Regression(3-D)
Mean Error of x (m)	0.015	0.023	0.114	0.062	0.102
Mean Error of y (m)	0.014	0.022	0.123	0.066	0.116
Mean Error of z (m)	0.024	0.077	0.353	0.232	0.346

proposed method, a flexible moving window is designed to decrease the computation shown in Fig. 5. Each edge in the graph can be regarded as a constrained equation shown in Fig. 2. So for single robot localization, each position has three constrained equations(except at the start and end position). Another important parameter is the maximum number of iterations for the optimization algorithm on Lie-Manifold presented

in Section V.

In our localization system, the maximum velocity of UAV is $2m/s$, and the update rates of IMU and UWB are $100.3Hz$ and $32.46Hz$, respectively. The effects of the maximum number of constrained equations and maximum number of iterations on localization are analyzed on $2.2GHz$ intel core i7 processor. The statistics of estimation error and update speed

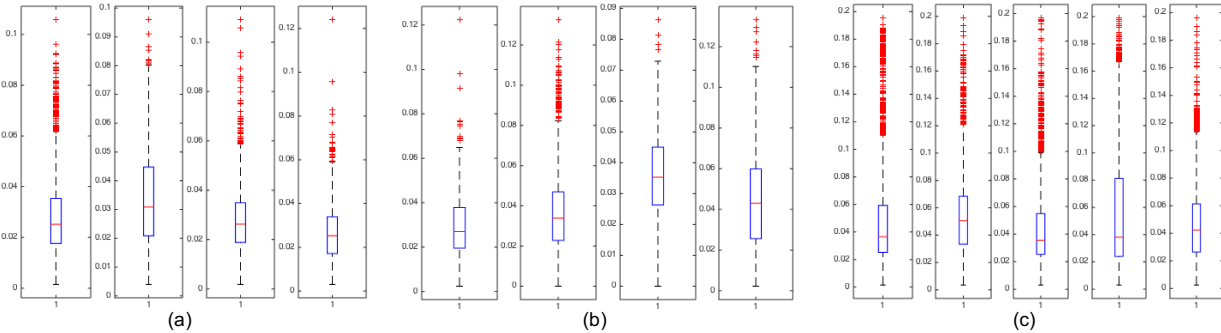


Fig. 11. Box figures of experiment results in 2-D and 3-D space.

with maximum 10 or 20 iterations in 2-D space are shown in Table 2 and Table 3. From Table 2, we can know that the update rate of localization is close to or higher than that of UWB (32.46Hz), when the maximum number of positions in the moving window are within 200. In this situation, the mean error of translation in (51) is within 3.4 centimeters. Some UWB measurements can not get into the moving window when the update rate of localization is much lower than that of UWB, then the mean error of translation estimation becomes greater (4.4 centimeters with 300 positions in the moving window).

Better localization results in 2-D space are obtained if the maximum number of iterations is set to 20 shown in Table 3. The proposed algorithm has the same accuracy (2.8 cm of mean error of translation) when the maximum number of measurements in the moving window are within 100. This is to say, when the update rate of the proposed algorithm is close to or higher than that of UWB, the localization accuracy will not be influenced. The mean error of translation estimation becomes greater (9.1 cm with 200 positions in the moving window) when the update rate of the proposed algorithm is much lower than that of UWB. Similar localization results in 3-D space are shown in Table 4.

When applied to Raspberry Pi, the maximum number of iterations is set as 10 iterations and window size is taken as 10. In this case, we can have an updated rate of about 33.2Hz which is higher than that of UWB. For the parameters of covariance matrices, Ω_i^r in (15) and Ω_i^o in (22) are provided by UWB and IMU sensors directly. The penalty term w_i^c is chosen according to (17) and (23).

TABLE II
TRANSLATION ERROR VERSUS UPDATING WINDOW SIZE UNDER THE
MAXIMUM NUMBER OF ITERATIONS OF 10 IN 2-D SPACE

Window Size	10	25	100	200	300
Mean Error(m)	0.032	0.033	0.034	0.033	0.044
Standard Deviation(m)	0.018	0.019	0.018	0.018	0.028
Update Rate(Hz)	418.8	158.9	53.44	28.05	20.42

C. Comparison with Existing Methods

In the comparison with existing methods, the same devices and same experimental environment are guaranteed. The existing methods are our lab methods presented in [12], [18].

TABLE III
TRANSLATION ERROR VERSUS UPDATING WINDOW SIZE UNDER THE
MAXIMUM NUMBER OF ITERATIONS OF 20 IN 2-D SPAC

Window Size	10	20	50	100	200
Mean Error(m)	0.028	0.028	0.028	0.028	0.091
Standard Deviation(m)	0.017	0.018	0.017	0.018	0.037
Update Rate(Hz)	242.6	140.1	63.54	30.58	16.52

TABLE IV
TRANSLATION ERROR VERSUS UPDATING WINDOW SIZE UNDER THE
MAXIMUM NUMBER OF ITERATIONS OF 20 IN 3-D SPACE

Window Size	10	20	50	100	200
Mean Error(m)	0.067	0.067	0.067	0.069	0.167
Standard Deviation(m)	0.068	0.066	0.067	0.068	0.098
Update Rate(Hz)	254.5	134.1	61.92	33.82	17.83

For the 18 experiments in 2-D space, 8 experiment results are chosen and shown in Fig. 9, where the ground truth and estimates are shown in red and blue, respectively. The results for the rest of the experiment are similar. The mean error and standard deviation of translation estimation are 3.3 and 1.7 centimeters, respectively.

For the 15 experiments in 3-D space, 5 experiment results are shown in Fig. 10. The comparison with EKF/UKF and nonlinear regression is presented in Table 1. The mean errors of our proposed algorithm in the x and y directions are about 2.3 and 2.2 centimeters and about 7.7 centimeters in the z direction, which are much more than the filter based localization methods which have a mean estimation error of about 6 to 12 centimeters in the x and y directions, and about 25 to 35 centimeters in the z direction.

The box figures of the estimation errors in 2-D and 3-D space are shown in Fig. 11. For 2-D localization, it is observed from Fig. 11(a) and Fig. 11(b) that about 75 percent of all estimation errors are within 4 centimeters. For 3-D localization, 75 percent of all estimation errors are within 8 centimeters as seen from Fig. 11(c). Therefore, our proposed method which integrates IMU with UWB measurements can provide much more localization than the existing EKF and UKF based approaches.

IX. CONCLUSION

In this paper, an ultra-wideband and IMU aided localization system was proposed based on a graphical optimization approach. The proposed algorithm does not require an kinetic model and can be implemented real-time on a ROS platform. It has a flexible moving window, which can be adjusted together with the number of maximum iterations to suit for the computing resource available. Compared with filter-based localization methods, better accuracy in 2-D plane and 3-D space is obtained, especially in the estimation of altitude. The high accuracy can be guaranteed, as long as the update rate of the algorithm is not less than that of UWB, which can be achieved through tuning the maximum number of iterations or the window size.

REFERENCES

- [1] J. Engel, T. Schöps, and D. Cremers, "LSD-SLAM: Large-Scale Direct Monocular SLAM," in *Computer Vision – ECCV 2014*. Cham: Springer International Publishing, 2014, pp. 834–849.
- [2] T. S. Jakob Engel and D. Cremers, "LNCS 8690 - LSD-SLAM: Large-Scale Direct Monocular SLAM," *European Conference on Computer Vision*. Springer, Cham, 2014.
- [3] T. W. J. M. A. J. D. Ankur Handa, "A Benchmark for RGB-D Visual Odometry, 3D Reconstruction and SLAM," *IEEE International Conference on Robotics and Automation (ICRA)*, 2014.
- [4] Z. Chen, H. Zou, H. Jiang, Q. Zhu, Y. Soh, and L. Xie, "Fusion of WiFi, Smartphone Sensors and Landmarks Using the Kalman Filter for Indoor Localization," *Sensors*, vol. 15, no. 1, pp. 715–732, Jan. 2015.
- [5] S. Sen, J. Lee, K.-H. Kim, and P. Congdon, "Avoiding Multipath to Revive Inbuilding WiFi Localization," *Proceeding of the th annual international conference on Mobile systems, applications, and services*. ACM, pp. 1–14, May 2013.
- [6] Z.-A. Deng, Y. Hu, J. Yu, and Z. Na, "Extended Kalman Filter for Real Time Indoor Localization by Fusing WiFi and Smartphone Inertial Sensors," *Micromachines*, vol. 6, no. 4, pp. 523–543, Apr. 2015.
- [7] S. Lupashin, M. Hehn, M. W. Mueller, A. P. Schoellig, M. Sherback, and R. DAndrea, "A platform for aerial robotics research and demonstration: The Flying Machine Arena," *Mechatronics*, vol. 24, no. 1, pp. 41–54, Feb. 2014.
- [8] A. Kushleyev, D. Mellinger, and V. Kumar, "Towards A Swarm of Agile Micro Quadrotors," *Autonomous Robots*, vol. 35, no. 4, pp. 287–300, 2013.
- [9] A. Ledergerber, M. Hamer, and R. DAndrea, "A Robot Self-Localization System using One-Way Ultra-Wideband Communication," *IEEE/RSJ International Conference on Intelligent Robots and Systems IROS*, pp. 3131–3137, Oct. 2015.
- [10] G. J. J. Blanco, O.-d.-G. A, and F.-M. J A, "Mobile Robot Localization based on Ultra-Wide-Band Ranging: A Particle Filter Approach," *Robotics and Autonomous System*, pp. 496–507, 2009.
- [11] N. A. Alsindi, B. Alavi, and K. Pahlavan, "Measurement and Modeling of Ultrawideband TOA-Based Ranging in Indoor Multipath Environments," *IEEE Transactions on Vehicular Technology*, vol. 58, no. 3, pp. 1046–1058, Mar. 2009.
- [12] K. Guo, Z. Qiu, C. Miao, A. H. Zaini, C.-L. Chen, W. Meng, and L. Xie, "Ultra-Wideband-Based Localization for Quadcopter Navigation," *Unmanned Systems*, vol. 04, no. 01, pp. 23–34, Jan. 2016.
- [13] D. Dardari, A. Conti, U. Ferner, A. Giorgetti, and M. Z. Win, "Ranging With Ultrawide Bandwidth Signals in Multipath Environments," *Proceedings of the IEEE*, vol. 97, no. 2, pp. 404–426, Mar. 2009.
- [14] M. W. Mueller and M. Hamer, "Fusing ultra-wideband range measurements with accelerometers and rate gyroscopes for quadrocopter state estimation," *IEEE International Conference on Robotics and Automation (ICRA)*, pp. 1730–1736, 2015.
- [15] R. Dalce and A. Van den Bossche, "Indoor self-localization in a WSN, based on Time Of Flight: Propositions and demonstrator," *International Conference on Indoor Positioning and Indoor Navigation (IPIN)*, 2013.
- [16] G. E. Garcia, L. S. Muppisetty, E. M. Schiller, and H. Wymeersch, "On the Trade-Off Between Accuracy and Delay in Cooperative UWB Localization: Performance Bounds and Scaling Laws," *IEEE Transactions on Wireless Communications*, vol. 13, no. 8, pp. 4574–4585, Mar. 2014.
- [17] A. Prorok and A. Martinoli, "Accurate indoor localization with ultra-wideband using spatial models and collaboration," *The International Journal of Robotics Research*, vol. 33, no. 4, pp. 547–568, Apr. 2014.
- [18] T. M. Nguyen, A. H. Zaini, K. Guo, and L. Xie, "An Ultra-Wideband-based Multi-UAV LocalizationSystem in GPS-denied environments," *The International Micro Air Vehicle Conference and Competition*, 2016.
- [19] B. Hepp, T. Nägeli, and O. Hilliges, "Omni-directional person tracking on a flying robot using occlusion-robust ultra-wideband signals," *IEEE/RSJ International Conference on Intelligent Robots and Systems*, 2016.
- [20] A. N. Bishop, B. Fidan, B. D. O. Anderson, K. Doğançay, and P. N. Pathirana, "Optimality analysis of sensor-target localization geometries," *Automatica*, vol. 46, no. 3, pp. 479–492, Mar. 2010.
- [21] S. Martínez and F. Bullo, "Optimal sensor placement and motion coordination for target tracking," *Automatica*, vol. 42, no. 4, pp. 661–668, Apr. 2006.
- [22] J. T. Isaacs, D. J. Klein, and J. P. Hespanha, "Optimal Sensor Placement For Time Difference of Arrival Localization," *Proceedings of the th IEEE conference on Decision and Control*, pp. 1–7, Dec. 2009.
- [23] A. Benini, A. Mancini, and S. Longhi, "An IMU/UWB/Vision-based Extended Kalman Filter for Mini-UAV Localization in Indoor Environment using 802.15.4a Wireless Sensor Network," *Journal of Intelligent & Robotic Systems*, vol. 70, pp. 461–476, Aug. 2012.
- [24] X. Feng, H. snoussi, and Y. Liang, "Constrained Extended Kalman Filter for Ultra-Wideband Radio based Individual Navigation," *17th International Conference on Information Fusion*, 2014.
- [25] A. UmaMageswari, J. J. Ignatious, and R. Vinodha, "A Comparative Study Of Kalman Filter, ExtendedKalman Filter And Unscented Kalman Filter ForHarmonic Analysis Of The Non-Stationary Signals," *International Journal of Science and Engineering Research*, vol. 3, no. 7, pp. 1–9, 2012.
- [26] A. Rai, K. K. Chintalapudi, V. N. Padmanabhan, and R. Sen, "Zee: Zero-Effort Crowdsourcing for Indoor Localization," *In Proceedings of the th Annual International Conference on Mobile Computing and Networking*, pp. 293–304, Jul. 2012.
- [27] M. Youssef and A. Agrawala, "The Horus WLAN Location Determination System," *In Proceedings of the IEEE Third International Conference on Mobile Systems, Applications, and Services*, pp. 205–218, 2005.
- [28] C. Forster, M. Pizzoli, and D. Scaramuzza, "SVO: Fast Semi-Direct Monocular Visual Odometry," *IEEE International Conference on Robotics and Automation (ICRA)*, 2014.
- [29] F. Endres, J. Hess, J. Sturm, D. Cremers, and W. Burgard, "3-D Mapping With an RGB-D Camera," *IEEE Transactions on Robotics*, vol. 30, no. 1, pp. 177–187, Jan. 2014.
- [30] J. Engel, V. Koltun, and D. Cremers, "Direct Sparse Odometry," *IEEE Transactions on Pattern Analysis and Machine Intelligence*, pp. 1–14, Apr. 2017.
- [31] T. Whelan, R. F. Salas-Moreno, B. Glocker, A. J. Davison, and S. Leutenegger, "ElasticFusion: Real-time dense SLAM and light source estimation," *The International Journal of Robotics Research*, vol. 35, no. 14, pp. 1697–1716, Jan. 2017.
- [32] R. A. Newcombe, D. Fox, and S. M. Seitz, "DynamicFusion: Reconstruction and Tracking of Non-rigid Scenes in Real-Time," *in IEEE Conference on Computer Vision and Pattern Recognition*, pp. 343–352, 2015.
- [33] C. Forster, M. Pizzoli, and D. Scaramuzza, "SVO: Fast Semi-Direct Monocular Visual Odometry," *in IEEE International Conference on Robotics and Automation*, pp. 15–22, 2014.
- [34] R. Mur-Artal, J. M. M. Montiel, and J. D. Tardos, "ORB-SLAM: A Versatile and Accurate Monocular SLAM System," *IEEE Transactions on Robotics*, vol. 31, no. 5, pp. 1147–1163, Sep. 2015.
- [35] K. Tateno, F. Tombari, I. Laina, and N. Navab, "CNN-SLAM: Realtime dense monocular SLAM with learned depth prediction," *arXiv.org*, p. arXiv:1704.03489, 2017.
- [36] D. DeTone and T. Malisiewicz, "Toward Geometric Deep SLAM," *arXiv.org*, p. arXiv:1707.07410, 2017.
- [37] C. Wang, L. Xie, and J. Yuan, "Non-Iterative Localization and Fast Mapping," *arXiv.org*, p. arXiv:1710.05502, Oct. 2017.
- [38] J. Aulinás, Y. Petillot, J. Salvi, and X. Llado, "The SLAM problem: a survey," *Proceedings of the conference on Artificial Intelligence Research and Development*, pp. 362–371, 2008.
- [39] J. Aspnes, T. Eren, D. K. Goldenberg, A. S. Morse, W. Whiteley, Y. R. Yang, B. Anderson, and P. N. Belhumeur, "A Theory of Network Localization," *IEEE Transaction on Mobile Computing*, pp. 1663–1678, 2006.

- [40] X. Wang, M. Fu, and H. Zhang, "Target Tracking in Wireless Sensor Networks Based on the Combination of KF and MLE Using Distance Measurements," *IEEE Transactions on Mobile Computing*, vol. 11, no. 4, pp. 567–576, Feb. 2012.
- [41] C. Di Franco, A. Prorok, N. Atanasov, B. Kempke, P. Dutta, V. Kumar, and G. J. Pappas, "Calibration-free network localization using non-line-of-sight ultra-wideband measurements," in *the 16th ACM/IEEE International Conference*. New York, New York, USA: ACM Press, 2017, pp. 235–246.
- [42] Y. Diao and Z. Lin, "A Barycentric Coordinate based Distributed Localization Algorithm for Sensor Networks," *IEEE Transactions on Signal Processing*, pp. 4760–4771, 2014.
- [43] U. A. Khan, S. Kar, and J. M. F. Moura, "DILAND: An Algorithm for Distributed Sensor Localization with Noisy Distance Measurements," *IEEE Transactions on Signal Processing*, pp. 1940–1947, 2009.
- [44] Y. T. Chan, W. Y. Tsui, H. C. So, and P. C. Ching, "Time-of-Arrival Based Localization Under NLOS Conditions," *IEEE Transactions on Vehicular Technology*, vol. 55, no. 1, pp. 17–24, Jan. 2006.
- [45] L. Cong and W. Zhuang, "Nonline-of-sight error mitigation in mobile location," *IEEE Transactions on Wireless Communications*, vol. 4, no. 2, pp. 560–573, Mar. 2005.
- [46] H. Chen, K. W. K. Lui, Z. Wang, H. C. So, and H. V. Poor, "Non-line-of-sight Node Localization based on Semi-Definite Programming in Wireless Sensor Networks," *IEEE Transactions on Wireless Communications*, pp. 1–5, Dec. 2009.
- [47] S. Venkatraman, J. Caffery, and H. R. You, "A Novel ToA Location Algorithm Using LoS Range Estimation for NLoS Environments," *IEEE Transactions on Vehicular Technology*, vol. 53, no. 5, pp. 1515–1524, Sep. 2004.
- [48] C. Hertzberg, "A Framework for Sparse, Non-Linear Least Squares Problems on Manifolds," *Master's thesis*, pp. 1–54, 2008.
- [49] C. Forster, L. Carbone, F. Dellaert, and D. Scaramuzza, "IMU Preintegration on Manifold for Efficient Visual-Inertial Maximum-a-Posteriori Estimation," *Robotics Science and Systems XI. No. EPFL-CONF-*, 2015.
- [50] E. Eade, "Lie Groups for 2D and 3D Transformations," 2013.
- [51] X. Longluo, L. Zhiliao, and H. WahTam, "Convergence analysis of the Levenberg–Marquardt method," *Optimization Methods and Software*, vol. 22, no. 4, pp. 659–678, Aug. 2007.
- [52] R. Kümmeler, G. Grisetti, and H. Strasdat, "g2o: A general framework for graph optimization," *IEEE International Conference on Robotics and Automation (ICRA)*, 2011.
- [53] M. Boutayeb, H. Rafaralahy, and M. Darouach, "Convergence analysis of the extended Kalman filter used as an observer for nonlinear deterministic discrete-time systems," *IEEE transactions on automatic control*, vol. 42, no. 4, pp. 581–586, 1997.



Chen Wang received the B.Eng. degree in electrical engineering from Beijing Institute of Technology (BIT), China, in 2014. He is currently pursuing the Ph.D. degree with the School of Electrical and Electronic Engineering (EEE), Nanyang Technological University (NTU), Singapore. He received the Best Paper Award from 2017 18th International Conference on Advanced Robotics (ICAR 2017). His research interests include robot perception and machine learning.

Xu Fang received the B.Eng. degree





Lihua Xie received the B.E. and M.E. degrees in electrical engineering from Nanjing University of Science and Technology in 1983 and 1986, respectively, and the Ph.D. degree in electrical engineering from the University of Newcastle, Australia, in 1992. Since 1992, he has been with the School of Electrical and Electronic Engineering, Nanyang Technological University, Singapore, where he is currently a professor and Director, Delta-NTU Corporate Laboratory for Cyber-Physical Systems. He served as the Head of Division of Control and Instrumentation from July 2011 to June 2014. He held teaching appointments

in the Department of Automatic Control, Nanjing University of Science and Technology from 1986 to 1989.

Dr Xie's research interests include robust control and estimation, networked control systems, multi-agent networks, localization and unmanned systems. He is an Editor-in-Chief for Unmanned Systems and an Associate Editor for IEEE Transactions on Control of Network Systems. He has served as an editor of IET Book Series in Control and an Associate Editor of a number of journals including IEEE Transactions on Automatic Control, Automatica, IEEE Transactions on Control Systems Technology, and IEEE Transactions on Circuits and Systems-II. He is an elected member of Board of Governors, IEEE Control System Society (Jan 2016-Dec 2018). Dr. Xie is a Fellow of IEEE and Fellow of IFAC.